Applied Physics Express **8**, 063003 (2015)
http://dx.doi.org/**10.7567/APEX.8.063003**

Curved geometrical confinement effect on vortex-state reversals in magnetic half-spheres

Myoung-Woo Yoo and Sang-Koog Kim*

National Creative Research Initiative Center for Spin Dynamics and Spin-Wave Devices, Nanospinics Laboratory, Research Institute of Advanced Materials, Department of Materials Science and Engineering, Seoul National University, Seoul 151-744, Republic of Korea
E-mail: sangkoog@snu.ac.kr

Received January 19, 2015; accepted April 21, 2015; published online May 14, 2015

We applied micromagnetic numerical calculations to a study of vortex-state reversal dynamics in half-spheres. We found an additional, heretofore unknown mechanism of vortex-core reversals that occur via the nucleation of a reversed vortex core at the edge of the half-sphere after expulsion of the original core either with or without the reversal of the original chirality, but without formation of the magnetization dip or Bloch point. The vortex-state reversals are affected by the curved geometrical confinement of the half-spheres. Detailed descriptions of the reversal dynamics offer the fundamentals of both vortex polarization and chirality reversals in curved restricted geometries.

Magnetization reversal dynamics in geometrically confined nanoscale magnetic elements has been intensively and extensively studied.[1–10] The main focus of these studies was the reversal dynamics of the magnetic vortex core in soft magnetic dots because of its fundamental relevance to the dynamic transformations of different topological solitons[2–10] and its potential applications in binary data-storage devices.[3,7] One of the vortex-core-reversal mechanisms found thus far is the creation of a vortex–antivortex pair with core magnetizations opposite to the initial vortex-core magnetization, followed by the annihilation of the original core together with the newly formed antivortex core.[3–5] The annihilation process is, in principle, accompanied by an exchange-energy explosion and subsequent spin-wave emission.[4,5] This reversal mechanism is of technological importance because it can be achieved, with low power consumption, by resonant excitations[5,6,8] of one of the vortex-gyration[11] and azimuthal spin-wave modes.[12] Another core-reversal mechanism in nanodisks driven by out-of-plane spin-polarized currents is the creation of coupled edge solitons without exchange-energy explosion and spin-wave emission.[9] In addition, radial spin-wave-mode-driven vortex-core reversals by perpendicularly oscillating magnetic fields[10] present the nucleation of a Bloch point at the surface of planar dots, followed by its displacement along the thickness.[2,10]

All of the above studies were restricted mainly to two-dimensional (2D) planar dots. Recently, advanced cutting-edge technologies have allowed the fabrication of more complicated three-dimensional (3D) nanostructures of a rich variety of shapes, including spheres,[13] half-spheres,[14] spherical shells,[15,16] and nanotubes.[17] Accordingly, 3D magnetic elements have attracted interest owing to their fundamental dynamic characteristics and potential applications in data-storage devices.[14]

Therefore, in this letter, we present our study on vortex polarization and chirality reversals in soft magnetic half-spheres with curved surfaces. We found a notable core-reversal mechanism that occurs with or without chirality switching, as mediated by curved-surface geometrical confinements, and which is different from vortex–antivortex pair and edge-soliton-mediated vortex-core reversal mechanisms found in soft magnetic planar dots. This reversal mechanism provides a reliable and efficient means of controlling both vortex core and chirality switching in a periodic array of half-spheres.

In the present study, we modeled a 3D permalloy (Py: $Ni_{80}Fe_{20}$) half-sphere of diameter $2R = 100$ nm and height $h = R$ [see Fig. 1(a)]. In the curved geometry and dimensions, competition between the long-range dipolar and short-range exchange interactions gives rise to the unique static vortex configuration shown in Fig. 1(b). The vortex structure in a ground state has upward core magnetization and counter-clockwise (CCW) in-plane curling magnetization around its core axis. To study the vortex-reversal dynamics in a given half-sphere, we employed finite-element micromagnetic numerical calculations. Specifically, we discretized the curved surfaces into triangles of roughly equal area using Hierarchical Triangular Mesh,[18] thereby preventing numerical errors incurred by irregularities. The dynamic motions of the magnetizations of the individual nodes (mesh size: ~4 nm) at the zero temperature were solved using the FEMME code (version 5.0.8),[19] which incorporates the Landau–Lifshitz–Gilbert equation.[20,21] The chosen Py material parameters were as follows: saturation magnetization $M_s = 8.6 \times 10^5$ A/m, exchange stiffness $A_{ex} = 1.3 \times 10^{-11}$ J/m, damping constant $\alpha = 0.01$, and zero magnetocrystalline anisotropy.

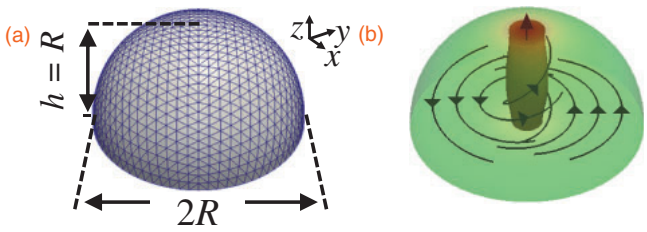

Fig. 1. (a) Model geometry of a half-sphere of diameter $2R = 100$ nm and $h = 50$ nm. (b) Ground vortex state of upward core magnetization and CCW in-plane curling magnetization.

To resonantly excite vortex-core motions, we utilized one of the excited modes in the half-sphere, the zeroth-order gyrotropic mode of eigenfrequency $\omega_0/2\pi = 1.5$ GHz.[22] Figure 2(a) is an illustration of an excitation of the zeroth-order gyration by a CCW circular-rotating field $\mathbf{H} = H_0[\cos(\omega_H t)\hat{\mathbf{x}} + \sin(\omega_H t)\hat{\mathbf{y}}]$ of field angular frequency ω_H and amplitude H_0, where $\omega_H = \omega_0 = 2\pi \times 1.5$ GHz and $H_0 = 100$ Oe. In this resonant excitation, the vortex core on the top curved surface shows a large-amplitude CCW orbiting motion, while on the bottom flat surface, it shows a small-amplitude CCW orbiting motion around its center position; therefore, the overall core is not vertically straight but rather largely bent.[22] The resultant trajectories of the resonantly excited gyrations on the top curved and bottom flat surfaces are presented in Fig. 2(b). The vortex-core position on the bottom surface was extracted using the maximum m_z value on the flat surface, while that on the top surface was extracted

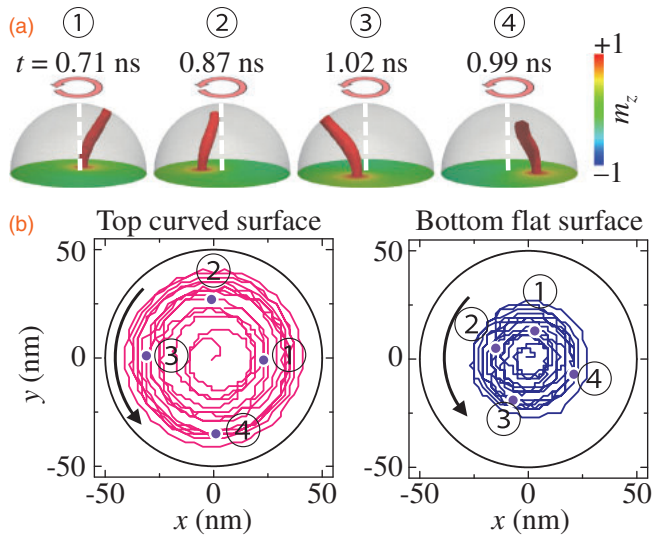

Fig. 2. (a) Snapshot images of vortex-core motion caused by resonant excitation of the gyration mode using a circular-rotating field in the CCW rotation sense and $\mathbf{H} = H_0[\cos(\omega_H t)\hat{\mathbf{x}} + \sin(\omega_H t)\hat{\mathbf{y}}]$, with $H_0 = 100$ Oe and $\omega_H/2\pi = 1.5$ GHz. The red pillars are displayed by the isosurface of $m_z = 0.9$, and the red wide arrow indicates the CCW rotation sense of the gyration of the vortex core. The colors at the bottom surfaces represent the local m_z distributions. (b) Trajectories of the gyration motion of the vortex core in the $t = 0$–5 ns time period at the top curved (left) and bottom flat (right) surfaces. Each dot on the trajectory curves indicates the position of the vortex core at the indicated moments, as noted by the numbers shown in (a).

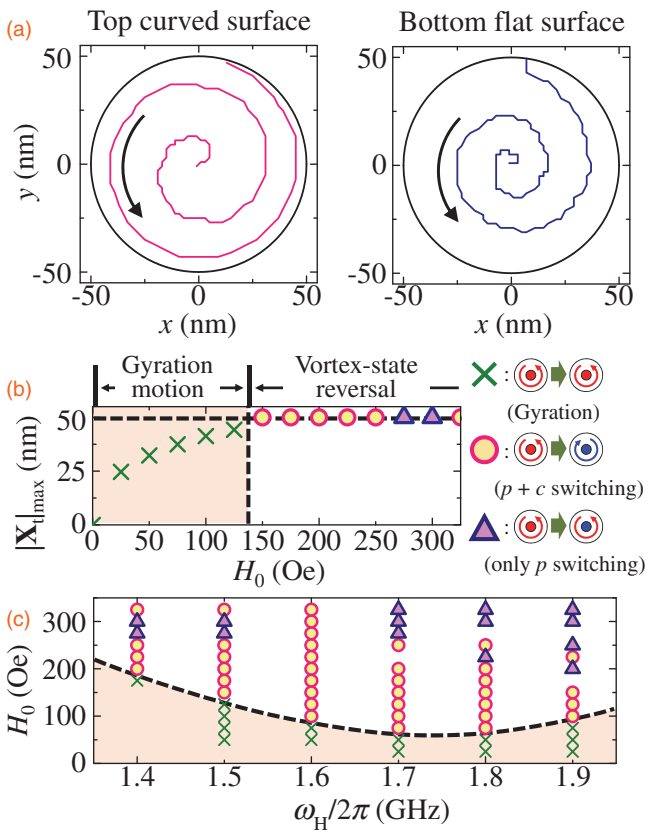

Fig. 3. (a) Trajectories of the gyration motion of the vortex core at the top curved (left) and bottom flat (right) surfaces up to core reversal, which was excited resonantly by the circular-rotating field of $H_0 = 150$ Oe and $\omega_H/2\pi = 1.5$ GHz. (b) Maximum orbit radius $|\mathbf{X}_t|_{max}$ of the core position on the top surface versus the rotating-field strength H_0 for $\omega_H/2\pi = 1.5$ GHz. (c) Phase diagram of vortex-state dynamics with respect to both H_0 and $\omega_H/2\pi$. In (b) and (c), the shaded regions correspond to the nonswitching case. In (c), the dashed curve is provided as a visual guide.

using the maximum value of $\mathbf{m} \cdot \hat{\mathbf{r}}$, where $\hat{\mathbf{r}}$ is the unit vector normal to the local surface. Both top and bottom trajectories show the same CCW rotation sense of the upward core gyration, but with a large difference in their orbit radii. The orbit radius at the top surface is about two times larger than that at the bottom surface, which consequently leads to the vertical core bending noted above.

As shown in Fig. 2, an H_0 of 100 Oe does not lead to core switching, because it is lower than the threshold-field amplitude. A further increase in H_0 to 150 Oe with $\omega_H/2\pi =$ 1.5 GHz allows for core gyration up to core reversal. In this core-reversal process, the vortex core on the top curved surface reaches the edge (the boundary between the top and bottom surfaces) of the half-sphere, as shown in Fig. 3(a). To determine when vortex-core switching occurs, we conducted further simulations by varying H_0 according to a given value of $\omega_H/2\pi = 1.5$ GHz. Figure 3(b) shows the plot of the maximum orbit radius ($|\mathbf{X}_t|_{max}$) of the vortex-core position at the top surface as a function of H_0. For $H_0 < 150$ Oe, $|\mathbf{X}_t|_{max}$ monotonically increases with increasing H_0, without any core-switching events. However, for $H_0 \geq 150$ Oe, the core position reaches a threshold orbit radius, i.e., the edge of the half-sphere [see Fig. 3(a)], and immediately thereafter the core magnetization is reversed. For $H_0 > 150$ Oe, the $|\mathbf{X}_t|_{max}$ values are the same, i.e., independent of H_0. This indicates that whenever the core position reaches the edge of the half-sphere, core reversals take place. In this heretofore unknown core-reversal mechanism, the core-reversal criterion is the curved geometrical confinement, i.e., the boundary between the top and bottom surfaces, as is discussed in detail below. There is another interesting dynamic behavior seen in this reversal mechanism: the core reversals take place with or without switching of the initial CCW chirality. For $H_0 \geq 150$ Oe, there are two different vortex dynamics that are unlike the core-reversal dynamics in 2D planar dots: simultaneous polarization and chirality switching [marked by the circle symbols in Fig. 3(b)] and only-polarization switching (marked by the triangle symbols).

Next, we examined the vortex dynamics versus the field frequency $\omega_H/2\pi$. Figure 3(c) is a phase diagram of the polarization, chirality switching, or both versus both the field frequency and the field strength. The threshold H_0 value, H_{th}, required for core switching varies with $\omega_H/2\pi$, as indicated by the dashed curve in Fig. 3(c). The minimum H_{th} value is ~75 Oe at $\omega_H/2\pi =$ ~1.7 GHz. This resonant field frequency is somewhat different from $\omega_0/2\pi = 1.5$ GHz. We assume that the 10% difference originates from the nonuniform thickness of the half-sphere when the core displacement increases. In the region between the H_{th} curve and $H_0 \sim 200$ Oe, there is simultaneous reversal of both the chirality and polarization, which is not observed in planar dots but only in cases where out-of-plane dc currents of extremely high current density are applied, as reported in Ref. 7.

To elucidate the difference and similarity of the underlying reversal mechanism in planar dots and half-spheres, we examined the details of the subprocesses of the polarization and chirality reversals [see Fig. 4(a) and the online supplementary data at http://stacks.iop.org/APEX/8/063003/mmedia]. Upon application of the rotating magnetic field, the

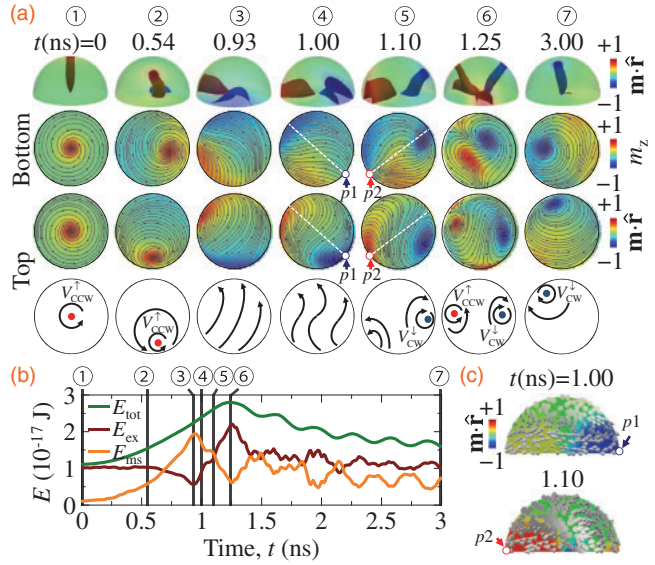

Fig. 4. (a) Serial snapshot images of the subprocesses of vortex polarization and chirality reversals in a half-sphere of diameter $2R = 100$ nm driven by a circular-rotating field of $H_0 = 200$ Oe and $\omega_H/2\pi = 1.5$ GHz. The first row shows the isosurfaces of $\mathbf{m} \cdot \hat{\mathbf{r}} = 0.8$ (red) and -0.8 (blue) in a perspectival view, while the second and third rows display the local magnetization distributions at the bottom flat and top curved surfaces, respectively. The open circles marked by "$p1$" and "$p2$" indicate the nucleation points of the downward and upward core magnetizations, respectively. The last row is a schematic of the local magnetization distributions at the top surface. (b) Temporal evolution of total (E_{tot}), exchange (E_{ex}), and magnetostatic energies (E_{ms}) during gyrotropic-mode-driven vortex-state reversal. (c) Spin configurations at the cross sections of dashed lines at $t = 1.00$ and 1.10 ns in (a), respectively. The white arrowheads indicate the orientations of the local magnetizations.

original upward core with CCW chirality ($V^{\uparrow}_{CCW}$) gyrates with increasing orbit radius ($t = 0$–0.90 ns). The core then disappears at $t = 0.90$ ns, when it reaches the half-sphere edge, resulting in a C-like magnetization configuration (see the images for $t = 0.93$ ns). At that point, the exchange (E_{ex}) and magnetostatic energies (E_{ms}) are at the local minimum and maximum, respectively, as shown by the temporal evolution of E_{ex} and E_{ms} in Fig. 4(b). Then, within $t = 1.00$–1.10 ns, a new core of downward magnetization with CW chirality ($V^{\downarrow}_{CW}$) is nucleated in a different region opposite the annihilation point, just after the original core is expelled from the half-sphere, to reduce the maximized E_{ms}. However, at this point, the overall chirality does not reverse completely (see the images for $t = 1.10$ ns). Immediately after the nucleation of the new downward core with CW chirality ($V^{\downarrow}_{CW}$) (i.e., at $t = 1.10$), another, new vortex core of upward magnetization with CCW rotation sense ($V^{\uparrow}_{CCW}$) begins to form spontaneously.[23] Thus, at this point, there are two vortex cores of opposite polarization and chirality on the top surface (see the images taken at $t = 1.25$ ns), which results in the highest value of E_{ex}, and, consequently, the attainment of the maximum total energy (E_{tot}) [see Fig. 4(b)]. However, the new upward core ($V^{\uparrow}_{CCW}$) is rapidly expelled to the opposite side ($t = 1.33$ ns), and then, finally, only the downward core with CW chirality ($V^{\downarrow}_{CW}$) remains in the half-sphere. These serial processes complete both the polarization and the chirality reversal (see the images taken at $t = 3.00$ ns).

These "polarization-plus-chirality reversal" subprocesses in half-spheres are quite different from those of edge–soliton-mediated core reversals in planar dots driven by out-of-plane dc currents. In the latter case, E_{ex} drops markedly when the original core is expelled from the given planar disk; so, for formation of the reversed new core inside the disk, the edge–soliton pair must overcome an E_{ex} barrier.[9] By contrast, in the case of the half-sphere, such a decrease in E_{ex} via annihilation of the original core is not observed ($t = 0.93$ ns) because of the half-sphere's curved surface. E_{ex} reaches its maximum value when two opposite vortex cores are formed inside the half-sphere ($t = 1.25$ ns); thus, it is of extremely high energy, as shown in Fig. 4(b). In addition, the origin of the new core's orientation differs from that for edge–soliton-mediated core switching, for which the core orientation is determined by the gyrofield at the nucleation site.[9] However, for the half-sphere, the magnetization direction at the nucleation site yields the nucleated core's orientation because of the geometrical curved surface. As shown in Figs. 4(a) and 4(c), because of the geometrical characteristics of the half-sphere, the magnetizations are normal to the curved top surface when $|\mathbf{m} \cdot \hat{\mathbf{r}}| = 1$ and the orientations are parallel to the upward or downward vortex core near the edge. Thus, to reduce the energy barrier to vortex-core formation, the inward [$\mathbf{m} \cdot \hat{\mathbf{r}} \sim -1$, marked as "$p1$" in Figs. 4(a) and 4(c)] and the outward ($\mathbf{m} \cdot \hat{\mathbf{r}} \sim +1$, marked as "$p2$") magnetization directions on the top surface at the edge correspond to the nucleation points of the downward and upward magnetization cores, respectively, unlike in edge–soliton-mediated core switching.[9] Consequently, in the case of the half-sphere, a new vortex core always forms at those points where the condition $|\mathbf{m} \cdot \hat{\mathbf{r}}| \sim 1$ is satisfied, and the formation of a new core is not caused by gyrofields, but rather by the magnetization direction at the edge of the half-sphere. This reversal mechanism, which differs from any mechanisms found in planar dots,[2–5,9,10] is driven by a specific nanoscale geometrical confinement. From further calculations, we observed that the "polarization plus chirality switching" also occurs in half-spheres of different size and in spherical caps with different wetting angles.[22,24] Such fine dynamic processes can be revealed only by 3D mesh-based numerical calculations. From an application point of view, both the polarization and the chirality reversals have an advantage in that they can be achieved with a relatively low field strength, i.e., ~100 Oe, when $\omega_H \sim \omega_0$. In planar dots, both reversals occur only when out-of-plane current densities larger than $\sim 10^8$ A/cm^2 are applied and a high-Oersted field is antiparallel to the initial chirality orientation.[7] We assumed that the small threshold-field amplitudes for chirality switching in the half-sphere originates from the spontaneous nucleation of the second core, despite the extremely high E_{ex}.[23]

We also found that in contrast to the above reversal mechanism, multiple chirality reversals added to the polarization reversal take place when $H_0 \gtrsim 200$ Oe. Figure 5 provides an example of such vortex-state reversal processes for $\omega_H/2\pi = 1.5$ GHz and $H_0 = 300$ Oe (also see the online supplementary data at http://stacks.iop.org/APEX/8/063003/mmedia). The overall reversal mechanism is almost the same as that of polarization-plus-chirality reversal, except for the inclusion of subprocesses ⑤ and ⑥, as shown in Fig. 5(a). Unlike the case of polarization-plus-chirality reversal, we observed an additional nucleation of the downward core with opposite chirality ($V^{\downarrow}_{CCW}$), after which the earlier $V^{\downarrow}_{CW}$ was expelled from the half-sphere and the $V^{\downarrow}_{CCW}$ remained as a

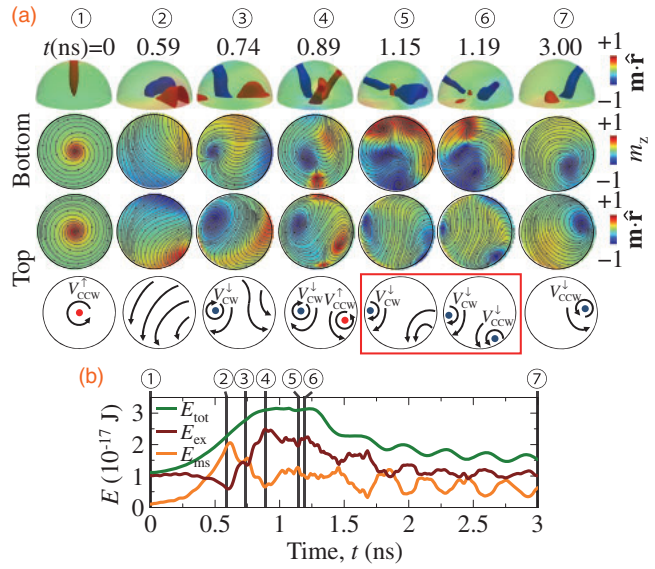

Fig. 5. Same as Figs. 4(a) and 4(b) except for the circular-rotating field strength of $H_0 = 300$ Oe applied for resonant excitation and the resultant only-polarization reversal.

new core without reversal of the original CCW chirality [see the images for $t = 3.00$ ns in Fig. 5(a)]. In the case of only-polarization switching, the reversal process is more complex than that in the polarization-plus-chirality reversal found in the $H_0 \lesssim 200$ Oe region, even though the mechanism of all the formations of the newly formed core's magnetization at the edge are the same as those shown in Fig. 4. The reversal processes in Fig. 5 are examples of the only-polarization reversal mechanism for cases of reversal when $H_0 \gtrsim 200$ Oe. For higher H_0 values, it is difficult to predict whether chirality reversals occur because there are multiple chirality reversals and additional complex nonlinear dynamics, as reported in Refs. 25 and 26. However, from a technological point of view, the only-polarization reversal mechanism is important because each vortex state can be independently switched to any of the other states through polarization-plus-chirality switching, only-polarization switching, or their combination, similar to the reliable control of any vortex states by application of out-of-plane currents to planar dots reported in Ref. 7. In future studies, it will be necessary to either find a way to prohibit such multiple chirality switching or to manipulate one-time switching to obtain another designated chirality in addition to vortex polarization switching in an array of half-sphere dots.

In summary, we studied vortex-state reversals in soft magnetic half-spheres using micromagnetic numerical calculations. We discovered an additional, unknown mechanism of vortex-state reversal, one that differs from those in planar dots. We observed fast polarization switching along with chirality switching driven by resonant excitations of the gyrotropic mode in the half-spheres and then clarified the reversal details with respect to the exchange and dipolar energy variations. The specific curved geometry of half-spheres affects the vortex-state reversals. Such detailed 3D dynamic features, unobtainable from numerical calculations for planar dots, offer both the fundamentals of and additional details on vortex-state reversals in curved-surface geometrical confinements. In addition, this work offers a guideline for experimental expectations of vortex-state reversals in arrays composed of half-spheres or sphere caps.

Acknowledgment This research was supported by the Basic Science Research Program through the National Research Foundation of Korea, which is funded by the Ministry of Science, ICT & Future Planning (Grant No. 2014001928). This work was also supported by the BK21PLUS SNU Materials Division for Educating Creative Global Leaders (Grant No. F15SN02D1702).

1) A. Huber and R. Schafer, *Magnetic Domains: The Analysis of Magnetic Microstructures* (Springer, Berlin, 1998).
2) A. Thiaville, J. M. Garcia, R. Dittrich, J. Miltat, and T. Schrefl, Phys. Rev. B **67**, 094410 (2003).
3) B. Van Waeyenberge, A. Puzic, H. Stoll, K. W. Chou, T. Tyliszczak, R. Hertel, M. Fahnle, H. Bruckl, K. Rott, G. Reiss, I. Neudecker, D. Weiss, C. H. Back, and G. Schutz, Nature **444**, 461 (2006).
4) R. Hertel and C. M. Schneider, Phys. Rev. Lett. **97**, 177202 (2006).
5) K. S. Lee, K. Y. Guslienko, J. Y. Lee, and S. K. Kim, Phys. Rev. B **76**, 174410 (2007).
6) V. P. Kravchuk, D. D. Sheka, Y. Gaididei, and F. G. Mertens, J. Appl. Phys. **102**, 043908 (2007).
7) Y. S. Choi, M. W. Yoo, K. S. Lee, Y. S. Yu, H. Jung, and S. K. Kim, Appl. Phys. Lett. **96**, 072507 (2010).
8) M. Kammerer, M. Weigand, M. Curcic, M. Noske, M. Sproll, A. Vansteenkiste, B. Van Waeyenberge, H. Stoll, G. Woltersdorf, C. H. Back, and G. Schuetz, Nat. Commun. **2**, 279 (2011).
9) K. S. Lee, M. W. Yoo, Y. S. Choi, and S. K. Kim, Phys. Rev. Lett. **106**, 147201 (2011).
10) M. W. Yoo, J. Lee, and S. K. Kim, Appl. Phys. Lett. **100**, 172413 (2012).
11) K. Y. Guslienko, B. A. Ivanov, V. Novosad, Y. Otani, H. Shima, and K. Fukamichi, J. Appl. Phys. **91**, 8037 (2002).
12) M. Buess, R. Hollinger, T. Haug, K. Perzlmaier, U. Krey, D. Pescia, M. R. Scheinfein, D. Weiss, and C. H. Back, Phys. Rev. Lett. **93**, 077207 (2004).
13) M. K. Kim, P. Dhak, H. Y. Lee, J. H. Lee, M. W. Yoo, J. Lee, K. Jin, A. Chu, K. T. Nam, H. S. Park, S. Aizawa, T. Tanigaki, D. Shindo, M. Kim, and S. K. Kim, Appl. Phys. Lett. **105**, 232402 (2014).
14) A. Samardak, E. Sukovatitsina, A. Ognev, M. Stebliy, A. Davydenko, L. Chebotkevich, Y. K. Kim, F. Nasirpouri, S. M. Janjan, and F. Nasirpouri, J. Magn. Magn. Mater. **371**, 149 (2014).
15) R. Streubel, V. P. Kravchuk, D. D. Sheka, D. Makarov, F. Kronast, O. G. Schmidt, and Y. Gaididei, Appl. Phys. Lett. **101**, 132419 (2012).
16) M. I. Sloika, V. P. Kravchuk, D. D. Sheka, and Y. Gaididei, Appl. Phys. Lett. **104**, 252403 (2014).
17) R. Streubel, J. Lee, D. Makarov, M. Y. Im, D. Karnaushenko, L. Han, R. Schafer, P. Fischer, S. K. Kim, and O. G. Schmidt, Adv. Mater. **26**, 316 (2014).
18) A. S. Szalay, J. Gray, G. Fekete, P. Z. Kunszt, P. Kukol, and A. Thakar, arXiv:cs/0701164.
19) D. Suess and T. Schrefl, FEMME: Finite Element MicroMagnEtics 5.0.8 (SuessCo) [http://suessco.com/].
20) L. D. Landau and E. M. Lifshitz, Phys. Z. Sowjetunion **8**, 153 (1935).
21) T. L. Gilbert, IEEE Trans. Magn. **40**, 3443 (2004).
22) M. W. Yoo, J. H. Lee, and S. K. Kim, J. Appl. Phys. **116**, 223902 (2014).
23) From further micromagnetic simulations in which the rotating field was turned off just after the first core ($V_{CW}^{\downarrow}$) nucleation, we found that the formation of the second core ($V_{CCW}^{\uparrow}$) is spontaneous, despite the extremely high E_{ex}, similarly to vortex–antivortex pair nucleation by the conventional core-switching process in planar thin nano-disks.
24) We performed similar micromagnetic numerical calculations with half-spheres of $2R = 80$ and 130 nm and spherical caps of $2R = 100$ nm and 70° wetting angle.
25) M. Kammerer, H. Stoll, M. Noske, M. Sproll, M. Weigand, C. Illg, G. Woltersdorf, M. Fahnle, C. Back, and G. Schutz, Phys. Rev. B **86**, 134426 (2012).
26) R. Hertel, S. Gliga, M. Fahnle, and C. M. Schneider, Phys. Rev. Lett. **98**, 117201 (2007).